YALE PEABODY MUSEUM

JOURNAL OF MARINE RESEARCH

The *Journal of Marine Research,* one of the oldest journals in American marine science, published important peer-reviewed original research on a broad array of topics in physical, biological, and chemical oceanography vital to the academic oceanographic community in the long and rich tradition of the Sears Foundation for Marine Research at Yale University.

An archive of all issues from 1937 to 2021 (Volume 1–79) are available through EliScholar, a digital platform for scholarly publishing provided by Yale University Library at https://elischolar.library.yale.edu/.

Requests for permission to clear rights for use of this content should be directed to the authors, their estates, or other representatives. The *Journal of Marine Research* has no contact information beyond the affiliations listed in the published articles. We ask that you provide attribution to the *Journal of Marine Research.*

Yale University provides access to these materials for educational and research purposes only. Copyright or other proprietary rights to content contained in this document may be held by individuals or entities other than, or in addition to, Yale University. You are solely responsible for determining the ownership of the copyright, and for obtaining permission for your intended use. Yale University makes no warranty that your distribution, reproduction, or other use of these materials will not infringe the rights of third parties.

Journal of
MARINE RESEARCH

The rise of bubbles in a glass tube and the spectrum of bubbles produced by a splash

by P. A. Bowyer[1]

ABSTRACT

Bubbles produced by a volume of 500 cc of water falling through a distance of 1.07 m into a water-filled basin were allowed to rise into an adjacent water-filled tube whose top was sealed at a level of 1.7 m above the level of water in the basin. The rise of these bubbles was recorded on video at a height of 1.5 m above the level of the splash: larger bubbles were recorded first. A model has been devised to describe the rise of such bubbles. The rise speed of the bubbles at the level of the video camera decreased with time after a splash, becoming nearly constant after a few minutes. The model used this long term rise speed to estimate the nitrogen saturation in the water. Oxygen saturation is measured by an electrode. Given the saturation it was then possible to use the model to calculate the initial spectrum of bubbles rising up the tube from the splash (i.e. the spectrum of such bubbles a second or two after the splash, when bubble fractionation or coalescence has ceased). The smallest bubble that could be seen depends on the gas saturation, but was typically of initial radius 20 μm, corresponding to a radius of 50–70 μm at the level of the video. Such spectra were found at different saturations, distances from the splash and salinities. At gas saturations of 105%–120%, a peak appears in the spectrum at a radius of about 20 μm. The time of admission of bubbles into the tube after a splash could also be restricted. For unrestricted sampling times, dN/dr varied as $r^{-1.5}$, when expressed as a power law. The spectrum above the peak value became steeper at later sampling times. At salinities below about 10 ppt, the number of bubbles of calculated initial radius < 600 μm is reduced. While no attempt was made to produce a realistic breaking wave, these results are relevant to attempts to define a source function of bubbles at sea, and to comparisons between fresh and salt water experiments.

1. Department of Oceanography, University College, Galway, Ireland.

1. Introduction

Bubbles may be important in air-sea gas transfer (e.g. Thorpe, 1982), or in the aggregation of particulates in the upper ocean (Johnson and Wangersky, 1986), or as vehicles for the transport of material to the surface microlayer (Wallace and Duce, 1975). In trying to model such processes, it is important to know the rate of input of bubbles into the surface ocean. A major source of near-surface bubbles in the ocean is the breaking of wind waves.

Several estimates have been made of the bubble concentration in splashes or whitecaps, and in adjacent water, both in the laboratory and at sea.

In the laboratory, Cipriano and Blanchard (1980) measured the concentration near a waterfall by drawing a sample of water into a parallel sided perspex chamber and photographing it. Medwin and Daniel (1990) measured acoustically the bubbles in a breaking wave in a tank and found a peak at a radius of 150 μm. Monahan (1988) has used the aerosol production by a breaking wave in a simulation tank to infer the flux of bubbles to the surface of the resulting whitecap and so to obtain an estimate of the near surface concentration of bubbles at sea. He did not find a peak in the spectrum. Baldy (1988), using holography, found that the spectral density of the concentration of bubbles in the water near breaking waves increased with decreasing size down to a radius of about 30 μm. Johnson (1986) used an underwater camera to measure the bubbles produced by a splash made by pouring water into a tank, finding the spectrum of bubbles of radius > 50 μm.

At sea, Blanchard and Woodcock (1957) measured the concentration of bubbles in the water near waves breaking over rocks and near the beach at Hawaii, and found a spectrum of slope −5. Kolovayev (1976) used a bubble trap to measure the bubble spectrum at sea in various wind conditions, which was also measured by Johnson and Cooke (1979) using an underwater camera. Both these studies revealed a peak in the size spectrum at radii of 50–100 μm. Bezzabotnov *et al.* (1986) measured the flux of bubbles to the surface photographically, and found a rapidly changing size spectrum: just after the breaking wave there was a peak at a radius of about 1.3 mm, but this value decreased rapidly in the few seconds after this. O'Hern *et al.* (1988) using a holographic method at sea found a large population of bubbles in calm conditions with a maximum near the thermocline.

Acoustic measurements include those of Medwin (1977), who measured the spectrum of bubbles in the sea and found considerable populations of bubbles even in the absence of breaking waves, and no peak in the bubble spectrum at radii down to 20 μm. He repeated and confirmed these measurements in 1989, and found the spectrum of bubbles in the water just after the passage of a spilling breaker to have a spectrum with a slope of about −2.7. Thorpe (1986) has used upwardly pointing side-scan sonar to measure the vertical distribution of bubbles in the ocean and found bubble clouds penetrating to a depth of up to 10 m, possibly reflecting the influence of Langmuir circulation.

The measurements described above are either measurements essentially of the concentration of bubbles (all acoustic measurements, as well as those of Johnson and Cooke, Cipriano and Blanchard, Baldy and O'Hern), or of the flux of bubbles into a bubble trap or through a surface (Blanchard and Woodcock, Kolovayev, Bezzabot-nov *et al.,* Monahan and this study). Both approaches have their problems: the spectrum of bubbles near a splash or whitecap changes rapidly with time and position, while the flux of bubbles of a given size into a trap (or to the surface) is a function of the rise speed of the bubbles, the circulation near the point of measure-ment, and the local concentration of the bubbles.

The smallest bubble that can be resolved varies widely. In the case of optical techniques, there may be a problem of distinguishing between very small bubbles and particles, especially if the bubbles have a thick coating of organic material, in which case they may not be spherical, or reflect light as normal bubbles. In the case of acoustic measurements, bubbles of less than 20 μm radius have resonant frequencies of > 150 kHz, and such sound is absorbed strongly by sea water, so that the detection of such bubbles is difficult (but possible). In the present study, the lower limit is very much dependent on the gas saturation in the water: any bubbles that expand (see Appendix) should be observed.

As for the larger bubbles, these are produced in smaller numbers, and most rise rapidly out of the water column in the vicinity of their production, so that they tend to be seen only in measurements which are made close to a breaking wave or splash. On the other hand, their size obscures the water behind them in photographic measure-ments, and can completely cover the surface of a bubble trap, leading to an underestimation of the number of smaller bubbles. In the present study, a region of surface was replaced with the bottom opening of the tube, and the separation of bubbles on the basis of rise speed that takes place in the tube allows more leisurely observation of both large and small bubbles.

In the few seconds immediately after a breaking wave or splash, when the concentration of bubbles is high, fractionation and coalescence of bubbles may occur in water of low salinity (Lessard and Ziemanski, 1971). The measurements described below (referred to as 'initial spectra') are of populations of bubbles which are left after such coalescence has ceased and which survive to rise into the tube.

2. Observations

a. The present study. In the present study, bubbles are produced by a splash in a shallow basin and rise through a water column to a point of observation at a level of about 1.5 m higher than the water level in the basin (Fig. 1). A model is used to calculate the time of rise and rise speed of bubbles at the point of observation. Both of these quantities are functions of the initial radius of the bubble and the gas saturation of the water.
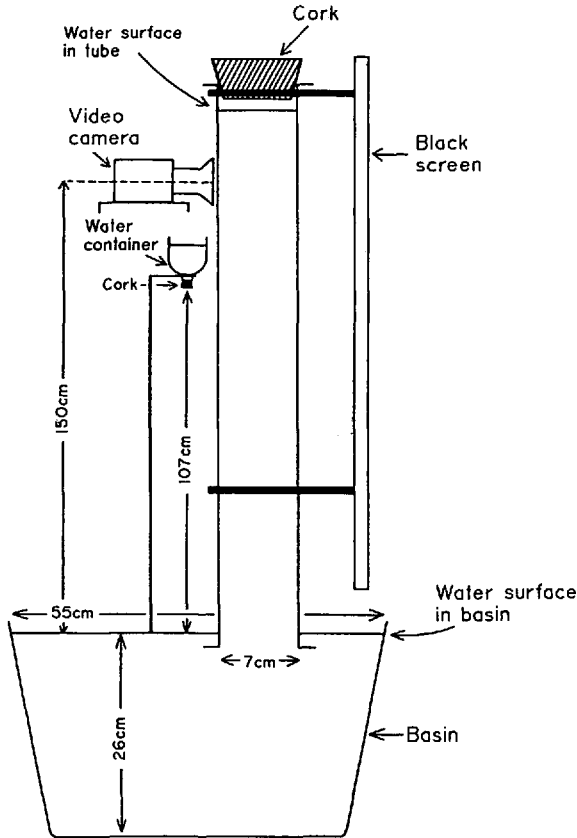
Figure 1. Apparatus.

The rise of single bubbles has been modelled following Thorpe (1982). Bubbles (assumed to be composed of nitrogen and oxygen in atmospheric proportions) are released at a specified depth (in this case 20 cm), and gas diffuses into or out of the bubbles as they rise through the water. The model uses a finite difference scheme: each timestep it calculates (a) the amount of gas entering or leaving the bubble, (b) the distance risen by the bubble and (c) the number of particles and amount of organic material captured by the bubble. The size, position and state of the bubble are updated for the next timestep. The length of the timestep is usually 1 s, but may be reduced in rapidly changing conditions such that the change in mole fraction of gas or bubble radius is never greater than 2% in one timestep. The diffusion occurs at a rate depending on the relative concentration of gas in the bubble and the water.

The partial pressure of gas (in this case, Nitrogen or Oxygen) inside the bubble is given by xP, where x is the mole fraction of the gas and P is the gas pressure inside the bubble, given by: $P = P_h + 2\gamma/a$, where P_h is the ambient pressure and $2\gamma/a$ is the Laplace pressured to the curvature of the bubble surface: γ is the surface tension and

a is the bubble radius. This term becomes important at small radii where it causes rapid dissolution of bubbles (see Appendix). P_h is given by $P_{at} + \rho gd$, where P_{at} is atmospheric pressure, d is the depth (negative in the tube above the level of water in the basin), g gravity and ρ the density of the water. The partial pressure of gas in the water in the water is given by $P_{at}Sx$, where S is the saturation and x is the mole fraction in air. The rate of diffusion of a gas is proportional to the difference in the partial pressure of the gas inside and outside the bubble, modified by a factor (the Nusselt number), which is expressed as in Thorpe (1982) as a function of the dimensionless Peclet number, aw/D, where w is the rise speed and D the gas diffusivity. Temperature dependent values of gas solubility and diffusivity, and water viscosity are used as described in Thorpe *et al.* (1992). The dependence of these quantities on salinity is less well known. Weiss (1970) found, for salinities of < 40 ppt, that the solubilities of Nitrogen and Oxygen were adequately represented by the Setchénow relationship (for a given temperature, $\ln(\beta) = b_1 + b_2S$, where β is the Bunsen coefficient, the b's are constants and S is the salinity in ppt). This relationship was assumed to be valid for higher salinities in the present study. The viscosity at high salinities was taken from the EDSU (1984) tables, and the Stokes Einstein equation ($D = kT/6\pi\mu a$) was used to derive the diffusivity in the absence of available data. The model uses the formulation of Clift *et al.* (1978) to derive the rise speed.

The model also calculated the number of particulates and amount of organic material captured by the bubble as it rises and is briefly described in Thorpe *et al.* (1992). Capture of organic material has the effect of immobilizing the surface of the bubble, and so reducing the surface tension of the bubble surface, the rise speed of and rate of diffusion of gas to the bubble (in which state the bubble is called 'dirty'). The flux of organic material to the bubble is calculated following Reay and Ratcliff (1973). In the conditions of this experiment, the model predicted that the bubbles became dirty on timescales of a second or less. Particles were captured by the mechanisms of shear (Hunt, 1980) and interception (Weber, 1981), of which the latter mechanism is the most important in these conditions. According to the model, at the particle concentration measured in the water used for this experiment, particulate capture significantly reduces the risespeed for $< 10\%$ of the bubbles and this conclusion was supported by observation (see results). For the rest of the bubbles in such conditions, the formulation of the model becomes essentially that of Thorpe (1982) for dirty bubbles in motionless water. The main problem with this model involved the treatment of the particulates and organic material: the efficiency of particle capture depends on the nature of the particles, and the capture of organic material depends on how much is surface active. However, in the present case, the particulate capture was low and the capture of organics high, so the bubbles behaved in a consistent manner, reflected in the small spread of the rise speeds observed at any given time for the majority of the bubbles. Bubbles which were significantly

affected by capture of particles will not be considered in this paper. No allowance was made for bubble-bubble interactions.

The aims of the study are twofold. Firstly to see whether the model can predict the relationship between the rise time and rise speed of bubbles. Secondly to use observations of the number and rise speed of bubbles at a known time after a splash to estimate the initial production of bubbles in the splash.

b. Apparatus. A glass tube about 1.7 m long and of 7 cm internal diameter (see Fig. 1), sealed with a rubber bung at the top and filled with water was suspended with its open bottom end 2 cm below the water surface in a basin of depth 26 cm. At a level of 150 cm above the water level in the basin, a video camera equipped with a macro lens was mounted with its lens against the side of the glass tube, so that the water in the middle of the tube was in focus, with a depth of field of 5 cm, and a field of view about 7 cm wide. The tube was held 3 cm from a black screen of width 15 cm and illuminated by a strip light positioned obliquely behind the screen. There was some distortion of the field of view by the curvature of the tube, but since the measured variables were number and rise speed in a direction along the tube, this was unimportant.

Splashes were made in the basin by releasing a known volume of water from a constant height (107 cm) from a container (the top half of a plastic bottle, inverted and clamped such that the center of the hole in the top (which had a diameter of 1.5 cm) was a known distance from the outside edge of the glass tube. To make a splash, the container was sealed with a rubber bung, and 500 ml of water from the basin was gently poured into it. After waiting 10 minutes or more for the bubbles in the container to rise to the surface, the cork was removed to allow the water in the bottle to fall onto the surface of the water in the basin, and so cause the splash. If the water is assumed to fall freely under gravity, it has an impact velocity of approximately 4.5 m/s and a kinetic energy of about 2.3 J. The jet was examined using the video and found to be continuous when it entered the water in the basin, a process which took about 0.1 s.

When a splash was made in the basin adjacent to the bottom of the tube, some of the bubbles from the splash which would otherwise have come to the surface, rose into the tube. The water pressure in the tube was below atmospheric, so at 100% gas saturation, gas diffused into the bubbles as they rose up the tube, and by the time they reached the level of the camera, they were clearly visible, if not as spheres, at least as bright specks of light against a dark background. If the initial depth of the bubbles is assumed, it is possible, knowing the rise speed and rise time of individual bubbles, to use the model to calculate their radius at the time of the splash and thus to get an idea of the initial size spectrum of bubbles rising into the tube.

Two sources of water were used in the experiment. The first source was tap water. To investigate the influence of salinity on bubble production, a nearly saturated
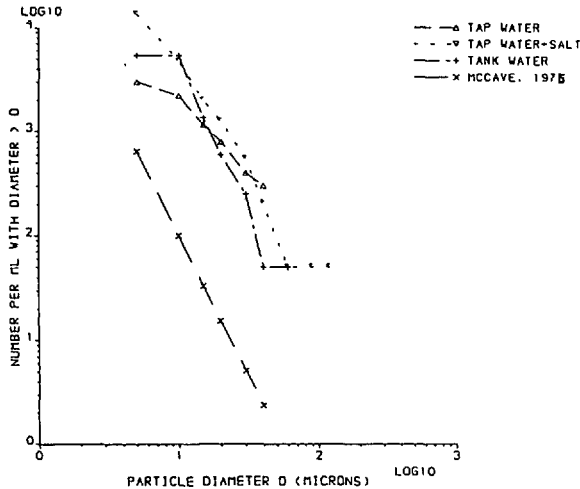
Figure 2. Particle concentration in the water, measured microscopically using a Sedgwick Rafter cell. Sources of water are explained in the text. McCave (1975) refers to the concentration of particles found in the upper layer of the ocean using a Coulter counter.

solution of brine was made up by dissolving salt in a bucket of fresh water. This was mixed thoroughly, covered and left to stand overnight in order to allow any bubbles produced by the mixing to rise out. Starting with fresh (tap) water, a quantity of brine of known salinity was mixed with the water in the tube and basin to give salinities between 0 ppt and 150 ppt. The second source was the water circulating in the aquarium system of the Oceanography Department of Southampton University, which has a salinity of about 32 ppt. Measurements of the particulate concentration of the water were made by counting the number of particles in a Sedgewick Rafter cell, and the concentration of particles of diameter $> 20 \ \mu m$ (see Fig. 2) was found to be about 20–50 times that measured by McCave (1975) at sea. The tube was cleaned before each set of (typically 10) splashes using tap water.

For these experiments, water of various gas saturations was used. At the start of a series of splashes, the water was usually slightly supersaturated. This was achieved by cooling the basin of water in a cold room at 5°C. for a period of several days, and then rapidly heating the water to room temperature (13–20°C). This usually resulted in a supersaturation of 5–15%. At supersaturations of $> 20\%$, there was a background flux of bubbles in the tube which made accurate counting difficult.

c. Method. Some 100 splashes were made. For about 60 of these, the distance between the outside of the tube and the center of the splash was about 2.5 cm. In the other splashes, this distance was changed to 10 or 17 cm (in which case, the tube was hard against the outer rim of the basin), and in this way, the variation of the flux with distance from, and so the total number of bubbles produced by, a splash could be measured.

For some splashes, the bottom of the glass tube was closed by a perspex 'trapdoor' which could be carefully slid into and out of position by hand, thereby restricting the time of admission of bubbles into the tube.

At the start of a series of splashes, the tube was filled by sealing the bottom and pouring water from the basin in through the top, which entailed the production of large numbers of bubbles, which usually took about 20 minutes to dissipate, after which the top was sealed and the bottom opened. After a splash or filling the tube, the number of bubbles in the field of view decreased with time, so by waiting a suitable length of time, it was arranged that the number visible prior to a splash was less than two for most saturations, and this meant that there was usually an interval of not less than 15 minutes between splashes. Oxygen saturation of water in the basin was measured using a WTW probe (accurate to about 2%) every second splash. This probe was also used to monitor water temperature and air temperature.

By way of comparison bubbles were allowed to rise onto a petri dish held in the water adjacent to the rise tube. After the bottom of the petri dish had been closed, it was lifted out of the water and placed on the stage of a microscope which was used to measure the bubble spectrum.

During and for a period of 10–15 minutes after a splash, the video camera recorded the bubbles rising past the point of observation at a height of 150 cm; the larger bubbles could be resolved, but bubbles of radius < 200 μm appeared as points of light. Levels were marked on the side of the tube at 6 cm intervals, so that the rise of individual bubbles could be recorded on the audio channel of the video. A group of bubbles was selected at a height of 25 cm above the water level, and if the relative position of the bubbles in the group changed by less than 3 mm as they rose through 6 cm, a bubble in the center of the group was chosen and whenever it passed a level mark, it was recorded verbally by the experimenter. Thus the rise time and rise speed of a few such individual bubbles were recorded as they rose through the tube.

3. Results

If the bottom of the tube is open at the time of a splash, the first bubble appears at the video camera about 5 s after the start of the splash. This may be a spherical cap bubble about 3–5 cm across. This is closely followed by many large bubbles rising erratically at about 10–20 cm/s. In the wake of each of these bubbles can be seen one or two smaller bubbles (whose radius was estimated to be about 200 μm). The size and rise speed of the bubbles in the field of view decreases with time and after about 20 s the bubbles are rising in straight lines with speeds consistent with their having risen from the level of the splash with almost constant velocity. After several minutes, the decrease in rise speed diminishes.

The rise speeds of the bubbles could be obtained easily by freezing the video picture at two times a known interval apart and tracing their positions onto a piece of acetate taped to the screen of the video monitor. If the rise speeds are plotted

(Fig. 3), they are generally found to be within 10% of some mean. Some objects are also seen with rise speeds considerably less than this mean, often associated with a visible particulate aggregation. These are bubbles which have captured particles large enough to significantly reduce their rise speeds. They constitute a small fraction (< 10%) of the total production of bubbles, and will not be considered in this paper. The numbers of bubbles were obtained either by freezing the frame (for the early, fast moving bubbles) or by counting the number crossing the screen in a given time (this was found to be easier for the later bubbles which usually had a smaller flux across the screen).

Figure 3 shows that the larger bubbles can be assumed to have risen at almost constant velocity, from positions at the time of the splash between 10 and 30 cm below the level of water in the basin. Assuming a depth of release of 20 cm, the model calculated the rise times to and rise speeds at the position of the video camera for bubbles with initial radii between 2 and 7000 μm. An example of the model output is shown in Figure 4, for fresh water at two different gas saturations. Above a threshold radius of 10 μm, for a saturation of 114%, (35 μm for a saturation of 102%) as the initial radius increases, the rise time decreases and the rise speed at the position of the camera increases. If the initial radius of the bubble is below this threshold, the Laplace pressure on the newly formed bubble will cause it to collapse within a few seconds after its formation, so such bubbles do not rise to the height of the video camera, and this defines the smallest bubble which can be detected by this technique (see the discussion below).

All the bubbles of initial radius greater than this threshold are easily detected by the video system, regardless of their initial size. For a given gas saturation (Fig. 4), the rise speeds of the bubbles at the camera change very slowly with changes of the initial radius below an initial value of ≈ 60 μm. This slow change is because these bubbles are expanding slowly as they rise through the tube, and the smaller bubbles, which take longer to rise, grow more than the larger bubbles, so that the differences in radius, hence rise speed, at the time of recording are quite small. However the rise time of the bubbles is sensitive to their initial radius.

The rise speed of the smallest bubbles is also weakly dependent on the initial depth of the bubbles, but depends strongly on the gas (i.e. nitrogen and oxygen) saturation of the water. For a given oxygen saturation the rise speed varies by 0.7 mm/s for a 1% change in nitrogen saturation near equilibrium, falling to 0.4 mm/s per 1% change at gas saturations of 115%. The oxygen saturation was measured with a probe (accurate to within 2%), but it was not possible at the time to measure the nitrogen saturation of the water, so the rise speed of the smallest bubbles, which was measurable to an accuracy of 0.2–0.5 mm/s, was used to estimate the nitrogen saturation to within about 1%. For salt water which had been made up from tap water and brine, in which the biological activity was presumably small, the calculated
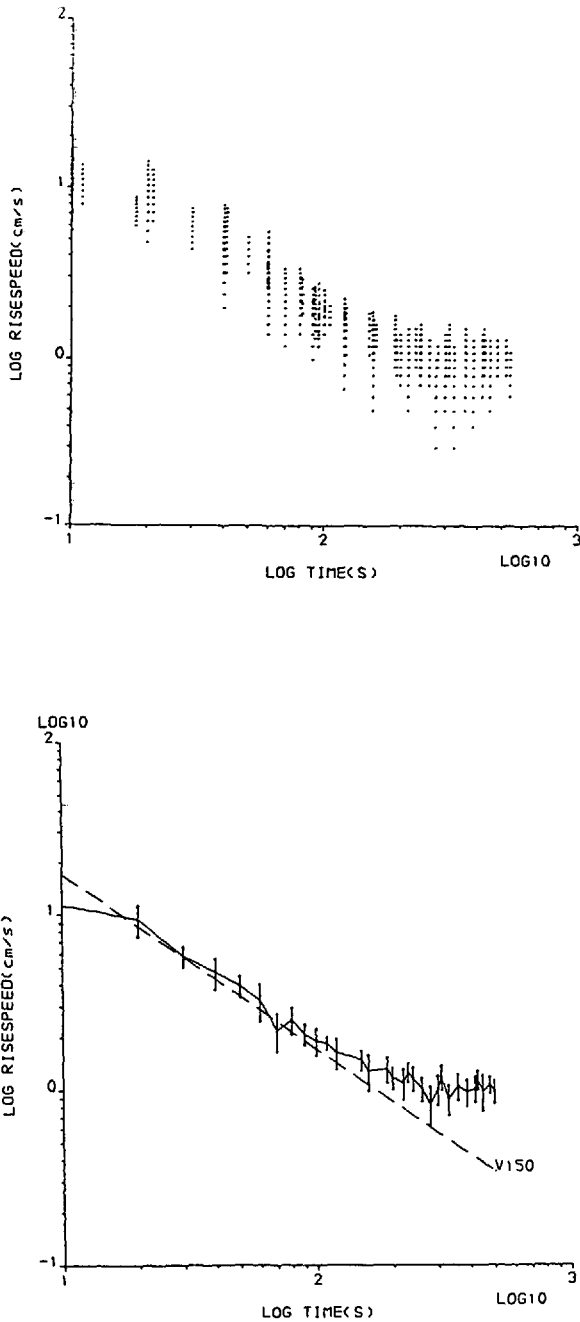
Figure 3. Rise speeds of bubbles passing the video, plotted against the time after a splash in water of gas saturation 105%. (a) scatter plot of individual measurements. (b) mean and standard deviation of measurements. Straight line ('V150') assumes bubbles rise with constant speed from a depth of 20 cm in the basin.
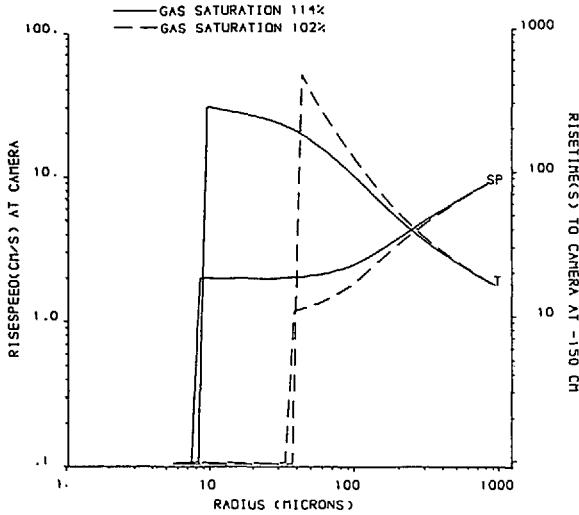
Figure 4. Output from the model. The rise speed (Sp) and rise time (T) of bubbles are plotted against their initial radius for fresh water of saturation levels (of both nitrogen and oxygen) of 114% and 102%. Note the insensitivity of the rise speed to radius at small radii. The threshold for detection is at 32 μm radius for 102% saturation and 9 μm for 114% saturation. Bubbles smaller than this dissolve before they reach the video. The risespeed of the smallest bubbles to rise up the tube is 1.1 cm/s at 102% saturation, and 2 cm/s for 114% saturation.

nitrogen saturation and the measured oxygen saturation always agreed to within 5%, usually to within 3%.

Once the gas saturation is known, it is possible to use the relationship between rise time (t_r) and initial radius (r_0) derived from the model to convert the observed relationship between numbers and rise times to a number-initial radius spectrum. Figure 5 shows a plot of the raw data, i.e. the number passing through the field of view versus the time after the splash, which can then be used to derive dN/dt_r versus t_r, and so the initial bubble size spectrum, dN/dr_0 using the relation $dN/dr_0 = (dN/dt_r)(dt_r/dr_0)$. It should be emphasized that N in this spectrum relates to all of the bubbles that rise into the tube during the time that the bottom of the tube is open.

The rise of individual bubbles through the tube is shown in Figure 6a as height-time curves. The observed curves and the predictions of the model (which used a gas saturation derived as above) are shown for several individual bubbles. Also shown (Fig. 6b) are the same data, with values of observed velocity plotted against predicted velocity.

Calculated initial spectra of bubbles entering the tube with no restriction on the time of entry are shown in Figure 7. These spectra are plotted as the number (per micron increment in radius) entering one square cm of the tube, in other words, the integrated flux through one square cm of surface. After a splash, bubbles smaller
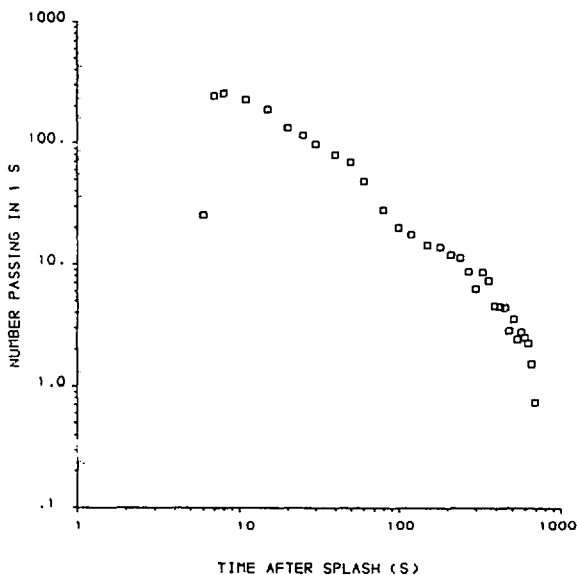
Figure 5. Raw data. A typical example of the flux of bubbles entering the video picture is plotted against the time after the splash. The salinity is 33 ppt and there is no restriction of the time of admission to the tube.

than a certain threshold dissolve quickly: the size of this threshold is sensitive to gas saturation (see Appendix). In the case of 15% gas supersaturation, bubbles of initial radius of $< \approx 15$ μm can be detected (by the time they reach the video, their radius is nearer 100 μm), and a peak in the spectrum appears to be present at a radius of ≈ 25 μm. If the gas saturation is less than this, these very small bubbles cannot be detected, so no peak is seen. The slope of the spectrum for radii > 30 μm is about -1.5.

Calculated initial spectra of bubbles entering the tube with restricted time of entry are shown in Figure 8. It can be seen that as the time of admission increases, the spectrum is cut off at progressively smaller radii, presumably because all of the larger bubbles have surfaced at this stage. Figure 9 shows two samples which were taken with the Petri dish adjacent to the tube and open for a similar time interval. There is reasonable agreement between the tube-derived spectra and the spectra found when bubbles on the Petri dish were counted microscopically. The water in this case had an oxygen saturation of 90%, so bubbles of radius < 35 μm were dissolved before they could rise up the tube. A few bubbles of radius < 15 μm were found on the Petri dish, mostly associated with particulate aggregation. The radius of these bubbles did not decrease for several hours after the measurement, and it is possible that they rose onto the Petri dish while they were still shrinking, and became stabilized there, as was observed by Johnson and Cooke (1980). Bubbles on the Petri dish were counted less than 5 minutes after a splash; the size of individual bubbles changed by $< 10\%$
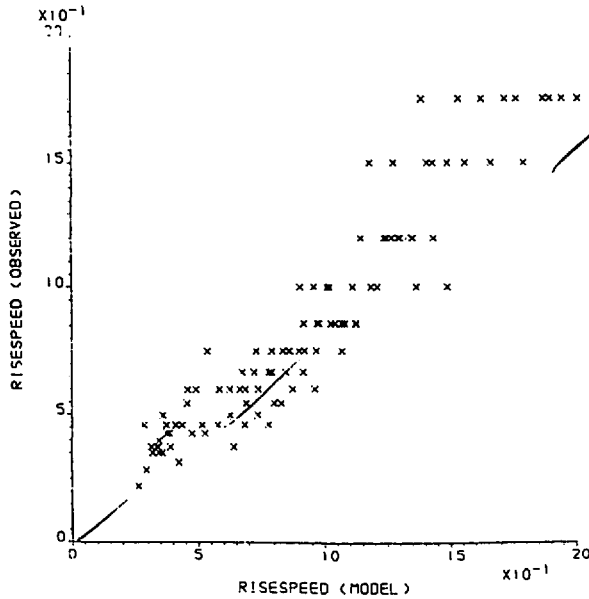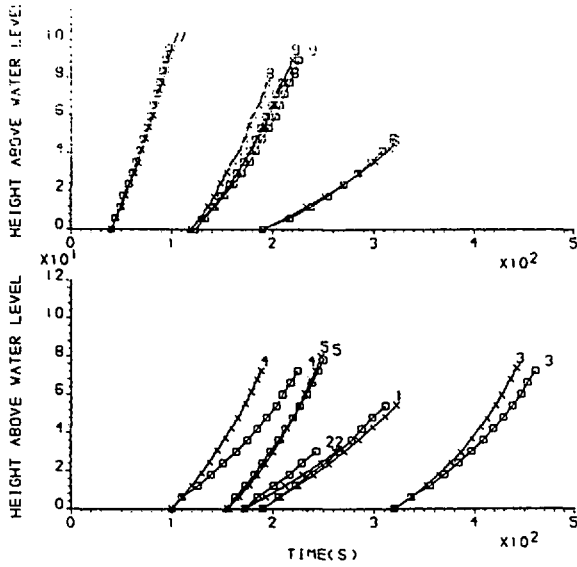
Figures 6. Comparison of observations and model results. (a) Height of individual bubbles as they rise through the tube plotted against time after splash. Measured values-squares; values predicted by the model-triangles. These measurements were made for bubbles at nitrogen saturations of between 100 and 120%. (b) Rise speeds (cm/s) of the individual bubbles in Figure 6a. Measured values plotted against values derived from the model.
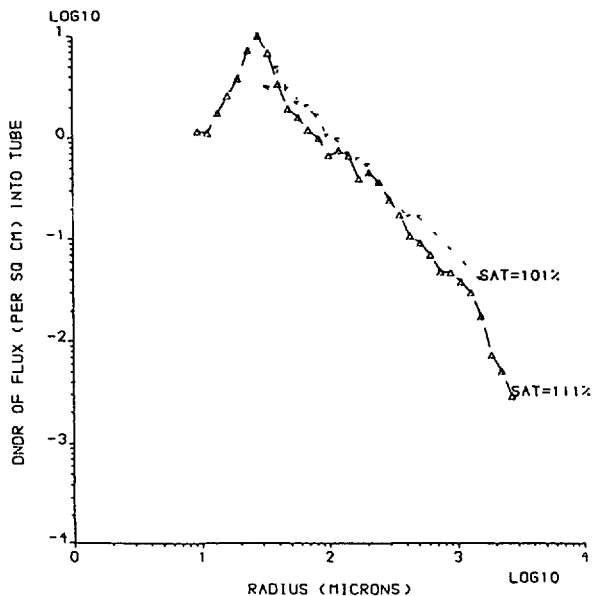
Figure 7. Calculated initial spectra of bubbles rising into the tube for two values of nitrogen saturation. The splash was 2.5 cm from the edge of the tube. At a saturation of 115%, the threshold for detection is about 10 μm. The oxygen saturation was within 3% of the nitrogen saturation.

after 20 minutes, so it is probable that the size of the bubbles when they were counted was similar to their size on sampling.

The effect of salinity is shown in Figures 10 and 11. Two sets of splashes were made. In the first set, the position of the tube was held at 2.5 cm from the center of the splash and the salinity varied between 0 and 150 ppt. Figure 10 shows the flux of bubbles (cm^{-2}). In the second set, the position of the tube was varied as explained above, so that estimates of the total number of bubbles produced by splashes at salinities between 0 and 50 ppt could be obtained. The variation of the bubble spectra with distance of the splash from the tube is shown in Figure 12 for fresh water. Bubbles of radius >200 μm are absent in position 3 (in which the distance of the splash from the edge of the tube, d, was 17 cm). Some bubbles with radii as large as 3 mm appear at position 2 ($d = 10$ cm), but a large peak appears in the spectrum of bubbles of radius >600 μm for position 1 ($d = 2.5$ cm). In this position, the numbers of bubbles of all radii are significantly larger than in positions 2 and 3.

If the time of entry is unrestricted, the number of small bubbles appears to be about 20 times less for fresh water than for 10 ppt water, although such bubbles are by no means completely absent in fresh water. There is a second peak in the fresh water spectrum for bubbles of radius >600 μm, and the numbers of such bubbles in fresh water are approximately equal to the numbers in salt water. For both sets of
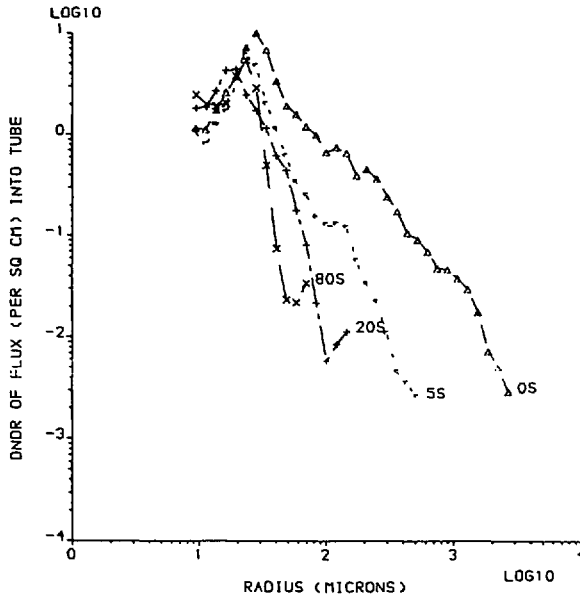
Figure 8. Calculated initial spectra of bubbles rising into the tube for different times of admission after a splash. The time (S) refers to the time in seconds after the splash at which the bottom of the tube was opened.
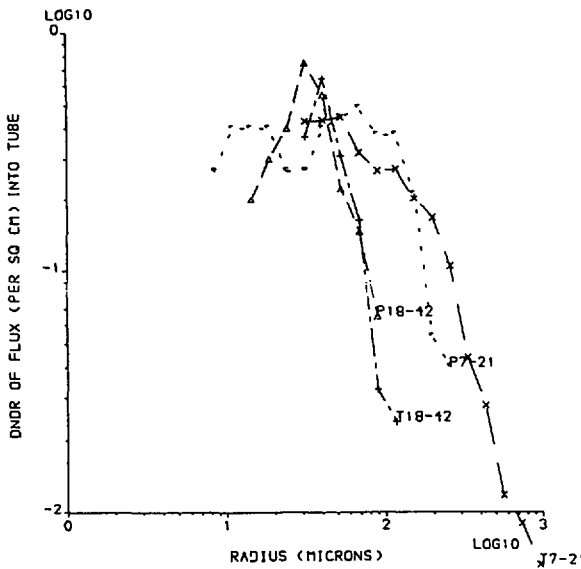

Figure 9. Comparison of the calculated initial spectrum of bubbles rising into the tube and the population rising onto a Petri dish and counted microscopically. Two sample intervals are shown: 7–21 s and 15–40 s.
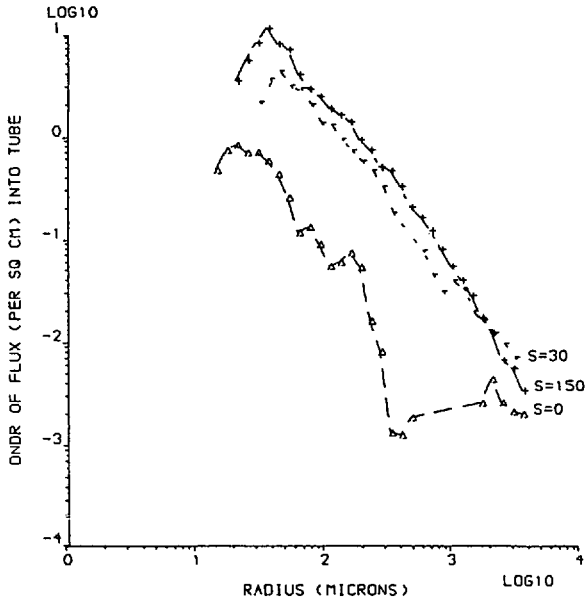
Figure 10. Calculated initial spectra of the bubbles entering the tube at 3 salinities. The splash was 2.5 cm away from the edge of the tube.
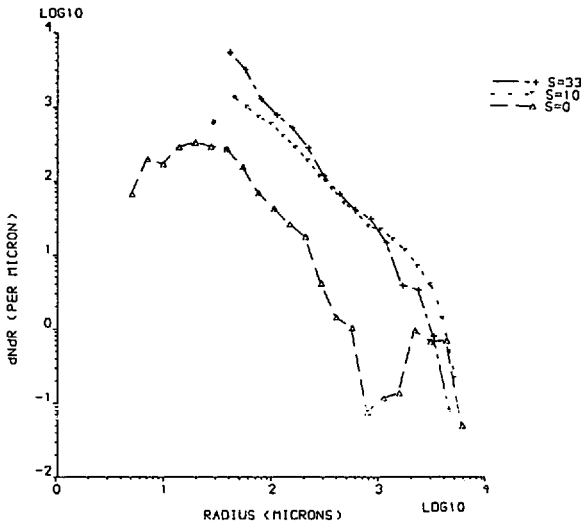

Figure 11. Calculated initial spectra of bubbles from a splash at different salinities. These spectra were obtained by integrating over the width of the basin.
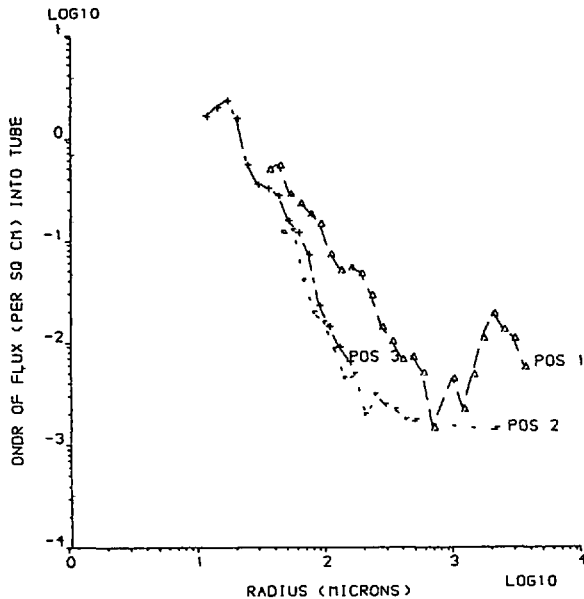
Figure 12. Calculated initial spectra of bubbles rising into the tube from a splashes at 3 different separations from the edge of the tube. POS 1: 2.5 cm; POS 2: 10 cm; POS 3: 17 cm separation between the centre of the splash and the edge of the tube.

splashes, there is little difference in the spectra for variations in salinity above 10 ppt. One difference that is apparent at these salinities is in the structure of the slug. At 150 ppt, the slug appears to have several attendant bubbles of radii 5–10 mm at its edge. These bubbles are possibly prevented from coalescing with the main slug by the high salinity.

The integrated volume of air entering the tube can be estimated from the decrease in water level in the tube after a splash. Typically, this is 3–5 mm for a splash adjacent to the tube in the case when a slug is allowed to enter the tube. The internal cross section of the tube has an area of 37 cm^2, giving a volume of 10–20 ml. The volume of the slug can be estimated by assuming cylindrical symmetry and tracing a cross section of the slug from the video. This varies between the limits 10–20 ml, depending on the splash. The volume of bubbles of radius smaller than 1 cm can be obtained from the spectra in Figure 11, and is found to be < 1 ml. Thus most of the entrained volume of air in the splash comes to the surface in < 5 s in the form of very large bubbles.

4. Dye experiments

In order to investigate the transport of water into the tube by large bubbles from a splash in salt water, a quantity of Rhodamine B dye was dissolved in the water in the basin, but not in the water in the tube. Two minutes after the splash, the bottom of
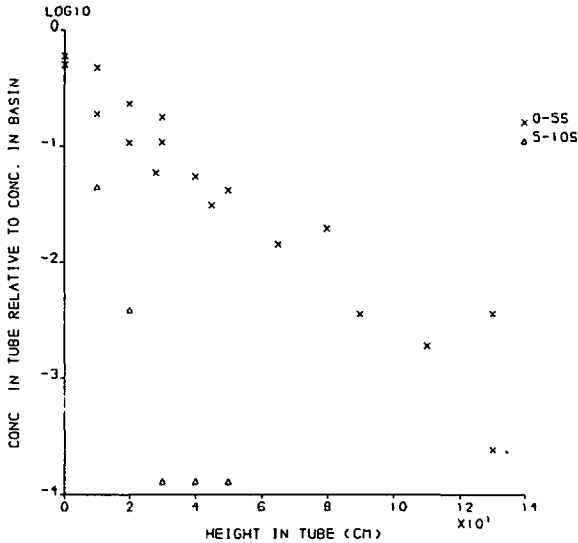
Figure 13. Concentration of Rhodamine dye in the tube (initially full of dye free water) after a splash 0–5 S-tube open from 0–5 seconds after a splash; 5–10 S-tube open between 5 and 10 seconds after a splash.

the tube was carefully sealed and the top opened and 10 ml samples were drawn off from various levels in the tube using a syringe to whose end 1.3 m of 1 mm internal diameter plastic tube was attached. The first sample was taken from the top of the tube, and subsequent samples were taken from positions progressively further down the tube, in order to avoid undue mixing due to the sampling process.

Three splashes were made, after each of which the tube was refilled with clear water. In two of the splashes bubbles were admitted into the bottom of the tube until 5 s after a splash, and in the third splash, the time of entry of the bubbles was restricted to between 5 and 10 s after the splash.

The concentration of dye in each sample was then measured using a Perkin Elmer LS5 fluorimeter. Profiles of dye concentration against vertical height in the tube are shown in Figure 13 for each of the splashes. The concentration of dye decreases exponentially with a lengthscale of about 25 cm for the 0–5 second splashes, compared with 2 cm for the 5–10 second splash. If the total amount of dye in the tube is calculated, it appears that in the former case, a piston of about 8 cm of water from the basin finds its way into the tube (i.e. 8 cm³ per cm² of surface) compared with about 1 cm in the latter case. This water is presumably carried in the wake of the bubbles and in the absence of the tube would represent a flux of water to the surface.

5. Discussion

Figure 3 shows that for rise times of < 100 s, the rise speed of bubbles at the level of the video camera are consistent with their having risen at constant velocity from a

depth of 20 cm in the basin (the assumed 'center of gravity' of the splash). For rise times longer than this, the rise speed of the bubbles is greater than could be expected. Such bubbles (of radius < 150 μm) must have expanded significantly (by the diffusion of gas from the water) as they rose through the tube. So if the model correctly represents the rise speed of the bubbles as a function of radius, the calculated bubble spectra for radii > 150 μm should be as accurate as the representation of risespeed. Below this radius, the model also needs to be able to represent the diffusion of gas accurately.

A major weakness of the present study is the inability to measure independently the nitrogen saturation of the water. Instead, this value is obtained by looking at the long term rise speeds of the bubbles, which is strongly dependent on the nitrogen saturation (oxygen saturation was measured by an electrode). If the paramaterization of the gas diffusion was wrong (Detsch, 1990), an erroneous value of nitrogen saturation would be obtained. This would reflect in the representation of the spectra of the small bubbles, as well as in the rise of individual bubbles shown in Figure 5. The level of agreement of the model and observations in Figure 5 would not be obtained if there was more than 30% error in the diffusion. An independent measure of nitrogen saturation could resolve this problem.

Any resemblance between the splashes producing bubbles in this experiment and any naturally occurring breaking wave is, of course, purely coincidental. Koga (1982), took photographs of bubbles generated by a jet impinging on a water surface, and found that the spectrum of bubbles was sensitive to the angle of attack of the jet; he suggested that a similar mechanism may be responsible for the entrainment of air by whitecaps on smaller waves. Whether or not a splash is a good representation of a whitecap, the rapid variation of the slope of the bubble spectrum (Fig. 8) indicates that most of the larger bubbles and entrained air in a splash may return to the surface very quickly, and probably the same holds for a plunging breaker at sea. Bubbles produced by whitecaps at sea are subject to transport from the surface by turbulence and organized water movement (e.g. Langmuir circulation), as well as being lost by dissolution and rising out. All of these factors are important in determining the evolution of such populations with time.

Cipriano and Blanchard (1980) measured the bubbles rising to the surface from a steady state salt water whitecap produced by a weir. They found a slope in the bubble spectrum of between −1 and −2, which is in rough agreement with the results presented here (Fig. 14). Furthermore, they found no bubbles of radius > 4 mm, which agrees with these measurements.

The effect of salinity on the bubble spectrum is marked for salinities below 10 ppt. Lennard and Ziemanski (1971) and Scott (1975) observed a similar phenomenon and accounted for it in terms of increased coalescence of bubbles in fresh water compared with salt water. This being so, processes which rely on the production of small bubbles by whitecaps, e.g. bubble mediated gas flux, can be expected to occur at
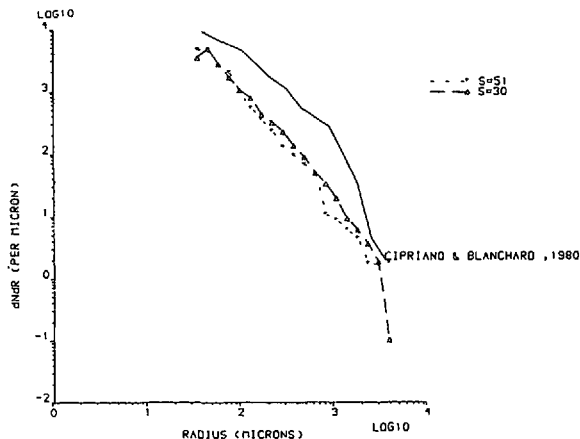
Figure 14. Calculated initial spectra of bubbles rising into the tube at salinities of 30 and 51 ppt, and data obtained in the vicinity of a laboratory weir by Cipriano and Blanchard (1980), replotted as dN/dr vs r.

different rates in salt and fresh water. At very high salinities, there seems to be a reduction of coalescence of bubbles as large as 1 cm diameter (see Section 4).

Most of the air entrained by the splash rises to the surface within seconds. In the tube this appears as a large slug of air. This slug grows very little as it rises up the tube and so it is formed as, or soon after, the leading bubbles enter the tube. Its rise speed is about 20 cm/s and this has probably been reduced by about 30% by the walls of the tube. Clift *et al.* (1978) have a plot of the rise speed of dirty bubbles as a function of bubble radius. There is a maximum in the rise speed at a radius of 1 cm and rise speed of 30 cm/s. Bubbles considerably larger than this near the surface would thus be overtaken by smaller, faster bubbles, possibly coalescing into a larger and slower bubble and this process may lead to the formation of a slug.

6. Conclusions

Referring to a standard splash made by dropping 500 ml of water from an orifice of 1.5 cm diameter a height of 107 cm above the water level:

1. For bubbles of radius r such that 3 mm $> r >$ 20 μm, the spectrum of bubbles produced by the standard splash in water of salinity > 10 ppt can be described as a power law $dN/dR = Ar^{-b}$, with $b = 1$–1.5 immediately after a splash, increasing to 3–5 s afterwards (see Section 3, and Fig. 7).

2. For water of salinity < 10 ppt, the number of bubbles of radius < 600 μm is lower than that found at higher salinities by a factor of up to 20 (Section 3, Fig. 12).

3. When water of oxygen and nitrogen saturation of 120% is used, a peak in the spectrum of bubble production appears in the region of 20 μm. Otherwise the saturation levels have little effect on the initial spectrum of bubbles (Section 3, Fig. 7).

4. The model predicts the rise time-rise speed relationship quite well, but the nitrogen saturation must be calculated by the model using the long term rise speed of the bubbles. There is quite good agreement between spectra of bubbles derived from the model and derived from measurements using a bubble trap.

5. Most of the bubbles (some 90%) do not have their rise speeds significantly slowed down by capture of large particles, even though the particle concentration is 20 times that observed by McCave (1975).

APPENDIX

Dissolution of small clean bubbles

Bubbles are assumed to be newly formed and clean. Further assuming the bubble (of radius a) to be composed entirely of nitrogen, the rate of change of radius can be expressed (Thorpe, 1982) as:

$$\frac{dp}{dt} = -\frac{1}{\left(3p + \dfrac{4\gamma}{a}\right)} \left\{ \frac{3RT}{a} \left[DKN \left(P_h + \frac{2\gamma}{a} - P_0 \right) \right] + a\frac{dP_h}{dt} \right\}$$

where D and K are the diffusivity and solubility of nitrogen in water, N is the Nusselt number (the increase of diffusion due to the movement of the bubble), γ is the surface tension (assumed to be that of a clean surface), S is the gas saturation (in %), P_h is the hydrostatic pressure near the bubble, P_0 is the partial pressure of gas in the water (I atmosphere at 100% saturation), R is the gas constant and T the absolute temperature.

The kernel of the diffusion term is

$$\left\{ P_h + \frac{2\gamma}{a} - P_{at} \frac{(S - 100)}{100} \right\}$$

. and this becomes negative (i.e. gas diffuses out of the bubble) if

$$P_h + 2\gamma/a > P_{at}(S - 100)/100.$$

The final term in the brackets, (the hydrostatic expansion due to the rise of the bubble) $= \rho a g w_d$ for a clean bubble of radius <80 μm, $\approx 3.10^{10}a^2$ in MKS, and this becomes less than the diffusion term if:

$$\frac{RTDKN}{a} \left\{ P_h + \frac{2\gamma}{a} - P_{at} \frac{(S - 100)}{100} \right\} > \rho a g w_d$$

i.e. if: $a < \approx 50$ μm for $S = 100\%$ near the surface.

If 1 μm $< a <$ 10 μm, the Nusselt number ≈ 1, the largest term in the pressure difference is $2\gamma/a$ which means that the gas diffusion term can be approximated by:

$$\frac{da}{dt} \approx \frac{2RT\gamma DK}{\rho a^2} \equiv \frac{\beta}{a^2}.$$

So, for clean bubbles of radius < 10 μm $a^3 = a_0^3 - \beta t$, and the bubble lasts for a time $t_l = a_0^3/\beta$. Substituting the expression for $a(t)$ into the equation for the rise speed, the distance risen by the bubble before it dissolves,

$$d_l < \frac{\beta g a_0^5}{3\nu}.$$

Thus, if it was not stabilized, a clean bubble of initial radius 10 μm would dissolve in about 10 s, having risen 3 mm through the water. For an initial radius of 1 μm, the bubble lasts about .01 s, having risen only 0.3 μm.

REFERENCES

Baldy, S. 1988. Bubbles in the close vicinity of a breaking wave. Statistical characteristics of the generation and dispersion mechanism. J. Geophys. Res., *93,* 8239–8248.

Bezzabotnov, V. S., R. S. Bortkovskiy and D. F. Timanovskiy. 1986. On the structure of the two phase medium formed when wind waves break, Isvestiya, Atmos. Ocean. Phys., *22,* 922–928.

Blanchard, D. C. and A. H. Woodcock. 1957. Bubble formation and modification in the sea and its meteorological significance. Tellus, *9,* 145–158.

Cipriano, R. and D. C. Blanchard. 1980. Bubble and aerosol spectra produced by a laboratory 'breaking wave.' J. Geophys. Res., *86,* 8085–8092.

Clift, R., J. R. Grace and M. E. Weber. 1978. Bubbles, Drops and Particles. Academic Press, 380 pp.

Detsch, R. M. 1990. Dissolution of 100 to 1000 μm diameter air bubbles in reagent grade water and seawater. J. Geophys. Res., *95,* 9765–9773.

Detwiler, A. and D. C. Blanchard. 1977. Aging and bursting bubbles in trace contaminated water, Chem. Eng. Sci., *33,* 9–13.

EDSU International Ltd. 1984. Validated engineering data index; package 77024.

Hunt, J. R. 1980. Prediction of oceanic particle size distributions from coagulation and sedimentation mechanisms, *in* Particulates in Water, M. C. Kavaunagh and J. O. Leckie, eds., Advances in Chemistry Series 189, 243–257.

Johnson, B. D. 1986. Bubble populations: background and breaking waves, *in* Oceanic Whitecaps and Their Role in Air-sea Exchange Processes, E. C. Monahan and G. MacNiocaill, eds., 69–73.

Johnson, B. D. and R. C. Cooke. 1979. Bubble populations and spectra in coastal waters: a photographic approach. J. Geophys. Res., *84,* 3761–3766.

—— 1980. Organic particle and aggregate formation resulting from the dissolution of bubbles in seawater. Limnol. Oceanogr., *25,* 653–661.

—— 1981. Generation of stabilized microbubbles in seawater. Science, *213,* 209–211.

Johnson, B. D., Xianling Zhou and P. J. Wangersky. 1986. Surface coagulation in sea water. Neth. J. Sea Res., *20,* 201–210.

Kolovyaev, P. A. 1976. Investigation of the concentration and statistical size distribution of wind produced bubbles in the near-surface ocean layer. Oceanology, *15*, 659–661.

Koga, M. 1982. Bubble entrainment in breaking wind waves. Tellus *34*, 481–489.

Lessard, R. R. and S. A. Zieminski. 1971. Bubble coalescence and gas transfer in aqueous electrolytic solutions, Ind. Eng. Chem. Fundam., *10*, 260–269.

McCave, I. N. 1975. Vertical flux of particles in the ocean, Deep-Sea Res., *22*, 491–502.

Medwin, H. 1970. *In situ* acoustic measurements of bubble populations in coastal ocean waters. J. Geophys. Res., *75*, 599–611.

—— 1977. *In situ* measurements of microbubbles at sea, J. Geophys. Res., *82*, 971–976.

Medwin, H. and N. D. Breitz. 1989. Ambient and transient bubble spectral densities in quiescent seas and under spilling breakers. J. Geophys. Res., *94*, 12751–12759.

Medwin, H. and A. C. Daniel, Jr. 1990. Acoustical measurements of bubble production by spilling breakers. J. Acoust. Soc. Am., *88*, 408–418.

Monahan, E. C. 1988. Near surface bubble concentration and oceanic whitecap coverage, *in* Oceanic Whitecaps and the Fluxes of Droplets from, Bubbles to, and Gases Through, the Sea Surface, Whitecap Report No. 4, Marine Sciences Institute, University of Connecticut, 178–181.

Monahan, E. C. and D. K. Woolf. 1988. A comprehensive model relating the marine aerosol population of the marine boundary layer to the bubble population of the oceanic mixed layer, *in* Oceanic Whitecaps and the Fluxes of Droplets from, Bubbles to and Gases Through, the Sea Surface, Report #4, Marine Sciences Institute, U. Connecticut, Groton, CT.

O'Hern, T. J., L. d'Agostino and A. J. Acosta. 1988. Comparison of holographic and Coulter Counter measurements of cavitation nuclei in the ocean. Trans. A.S.M.E., J. Fluids Eng., *110*, 200–207.

Reay D. and Ratcliff, G. A. 1973. Removal of fine particles from water bydispersed air flotation: Effects of bubble size and particle size on collection efficiency. Can J. Chem. Res, *51*, 178–185.

Scott, J. C. 1975a. The preparation of water for surface clean fluid mechanics, J. Fluid Mech., *69*, 339–351.

—— 1975b. The role of salt in whitecap persistence. Deep-Sea Res., *22*, 653–657.

Thorpe, S. A. 1982. On the clouds of bubbles formed by breaking wind waves in deep water, and their role in air-sea gas transfer. Phil. Trans. Roy. Soc. Series A, *304*, 155–210.

—— 1986. Measurements with an automatically recording inverted echo sounder; ARIES and the bubble clouds. J. Phys. Oceanogr., *16*, 1462–1478.

Thorpe, S. A., P. A. Bowyer and D. K. Woolf. 1992. Some factors affecting the size distributions of oceanic bubbles. J. Phys Oceanogr. *22*, 382–389.

Wallace, G. T. and R. A. Duce. 1975. Concentration of particulate trace metals and particulate organic carbon in marine surface waters by a bubble flotation mechanism. Mar. Chem., *3*, 157–181.

Weber, M. E. 1981. Collision efficiencies for small particles with a spherical collector at intermediate Reynolds numbers. J. Separ. Process Tech. *2*, 29–33.

Weiss, R. F. 1970. The solubility of nitrogen, oxygen and argon in water and seawater. Deep-Sea Res., *17*, 721–735.